In-situ investigation of deformation behavior and fracture forms of Ti/Al/Mg/Al/Ti laminates

Hui-hui NIE[1,2], Liu-wei ZHENG[3], Xiao-ping KANG[4], Xin-wei HAO[2,5], Xian-rong LI[2,5], Wei LIANG[2,3,5]

1. College of Mechanical and Vehicle Engineering, Taiyuan University of Technology, Taiyuan 030024, China;
2. Shanxi Key Laboratory of Advanced Magnesium-based Materials,
Taiyuan University of Technology, Taiyuan 030024, China;
3. Instrumental Analysis Center, Taiyuan University of Technology, Taiyuan 030024, China;
4. Shanxi Institute of Energy, Taiyuan 030006, China;
5. College of Materials Science and Engineering, Taiyuan University of Technology, Taiyuan 030024, China

Abstract: In-situ bending and stretching were conducted on hot-rolled and annealed Ti/Al/Mg/Al/Ti laminates, with a focus on crack initiation and propagation of intermetallics and component layers, which helps to clarify their deformation behavior and fracture forms. The results show that delamination is the early fracture form of laminate with or without intermetallics at Al/Mg interface, so Al/Mg interfacial bonding strength determines the mechanical properties of laminate. Various and irregular intermetallics cracks lead to Al/Mg interface delamination in annealed laminate and help to release stress. Necking and fracture of component layers are observed at the late deformation stage, and the sequence is Al, Mg and Ti layers, resulting from their strength. Angle between crack propagation direction and stretching direction of Mg layer both in rolled and annealed laminates is around 45° due to the effect of shear deformation, and crack convergence leads to final complete fracture of Mg layer.

Key words: Ti/Al/Mg/Al/Ti laminate; in-situ test; intermetallics; crack initiation; fracture form

1 Introduction

Mg alloy is a commonly used component sheet owing to its high specific strength and stiffness [1,2], and other metal sheets including Al, Ti, stainless steel, etc, are often cladded to the surface of Mg sheet by rolling, pressing, welding or extruding to obtain metal laminates [3−8]. These metal laminates have attracted much attention owing to their excellent comprehensive physical and mechanical properties [9,10].

Compared with single metal sheets, apart from the common failures including necking and fracture [11,12], metal laminates exhibit interfacial delamination in practice [13,14] because of the following reasons: (1) limited interfacial bonding strength of rolled or pressed metal laminates due to their layer-by-layer stacking nature [15,16]; (2) new intermetallics with high hardness and low ductility formed at a certain temperature during processing or application [17,18]. Therefore, interfacial delamination is an important failure form of metal laminates, which could significantly reduce the strength and stiffness of laminates. If microcracks at the interfaces or in component layers can be found at early stage of deformation, some industrial accidents can be prevented in advance. Therefore, it is of great importance to understand crack initiation and propagation process

of metal laminates.

In-situ scanning electron microscopy (SEM) investigation is a novel and effective method to detect crack initiation and propagation [19−21]. SADEGHI et al [22] studied the deformation behavior of steel/Mg/steel laminate using in-situ stretching, and clarified the relationship between fracture mode and slip activation by texture analysis of Mg layer at different strains [22]. In-situ stretching experiment of Al/Ti laminate indicates that ductile shear fracture is the main failure form of laminate rolled at low temperatures, while delamination is the main failure form of laminate rolled at high temperatures [23]. However, reports on crack initiation and propagation of Ti/Al/ Mg/Al/Ti laminate are few.

In this work, three-point bending and uniaxial stretching deformation process of Ti/Al/Mg/Al/Ti laminate were observed using in-situ SEM technique at room temperature. In order to obtain a comprehensive understanding of fracture mechanism of Ti/Al/Mg/Al/Ti laminate, two kinds of samples are prepared. One is rolled laminate, which focuses on the interfacial delamination, necking and fracture of component layers; the other is annealed laminate, which emphasizes on cracks of intermetallics themselves, and the effect of intermetallics on the failure of the whole laminate.

2 Experimental

2.1 Fabrication of Ti/Al/Mg/Al/Ti laminate

Commercial TA2 Ti, 5052 Al and AZ31 Mg were chosen as the component layers of Ti/Al/Mg/ Al/Ti laminate. After surface polishing and cleaning, these component layers were stacked and then rolled at 450 °C with a single pass of 50% rolling reduction. The specific rolling process has been

reported in our previous work [24]. Annealing temperature was 300 °C and the holding time was 1 h. Here, the rolled and annealed samples are denoted as R450 and A300, respectively.

2.2 In-situ tests and characterization

The dimensions of in-situ three-point bending and uniaxial stretching samples are given in Figs. 1(a) and (b), respectively. Before in-situ tests, samples were ground and polished. A Mira-3 SEM was used to observe the microstructure evolution of R450 and A300. In-situ deformation speed was set as 1 μm/s.

3 Results and discussion

3.1 Microstructures of Ti/Al/Mg/Al/Ti laminate

Figure 2 shows the microstructures of R450 and A300, both of which have well-bonded interfaces without delamination and voids. R450 presents a straight Ti/Al interface and a wavy Al/Mg interface, which is similar to three-layered Ti/Al/Mg laminates in our previous work [25]. A300 exhibits an obvious difference that two intermetallic layers appear at the Al/Mg interface. According to Mg−Al binary alloy phase diagram and literature [26], the layer near Al alloy is Al_3Mg_2 and the layer near Mg alloy is $Mg_{17}Al_{12}$.

3.2 In-situ bending test results

Figure 3 presents the whole three-point bending process of R450, and bending direction is marked in Fig. 3(a). The top Ti/Al and Al/Mg interfaces are chosen to investigate microstructure evolution, because top zone above the neutral layer of R450 undergoes tensile stress, which is easier to break than bottom zone under the compressive stress.

First, delamination locally happens at Al/Mg
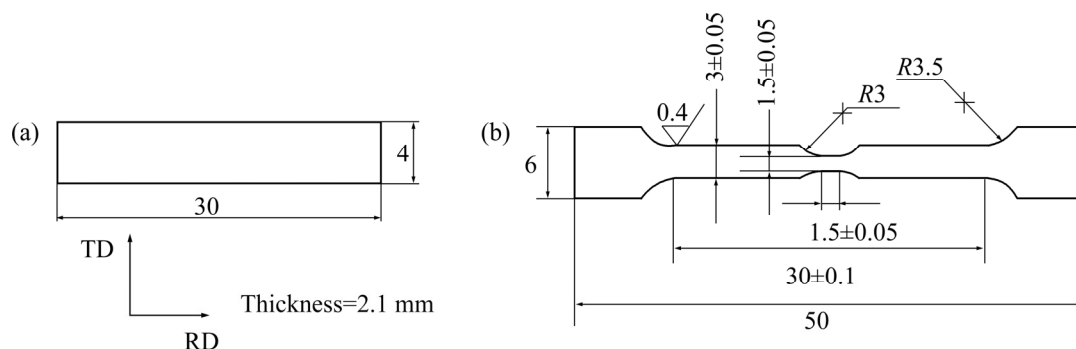
Fig. 1 Schematic of sample used in in-situ tests: (a) Three-point bending; (b) Uniaxial stretching (unit: mm)
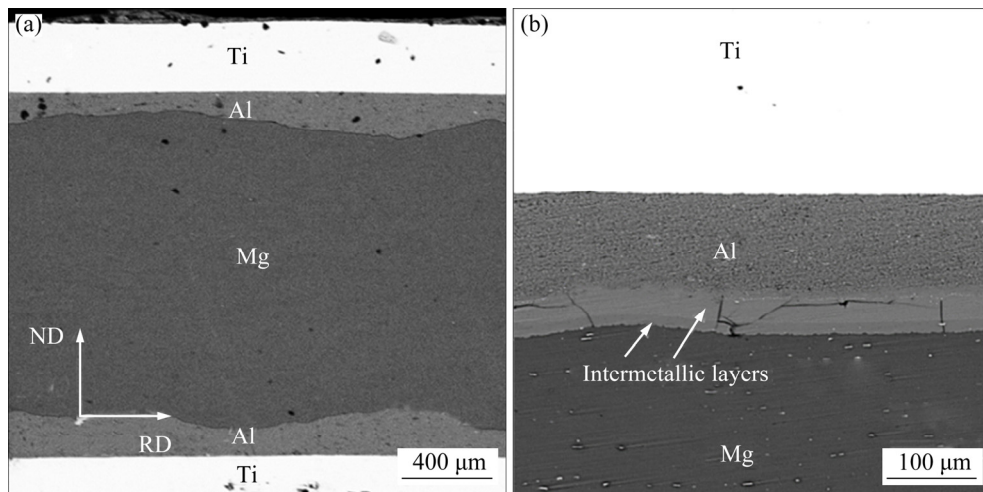
Fig. 2 Microstructures of Ti/Al/Mg/Al/Ti laminates: (a) R450; (b) A300
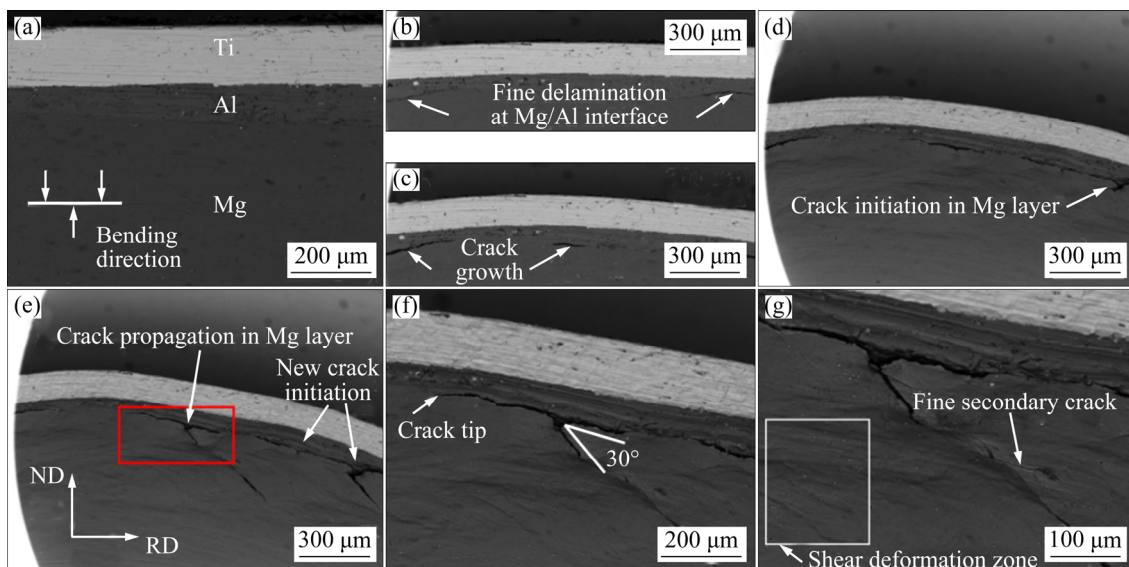
Fig. 3 Microstructure evolution of R450 during in-situ three-point bending

interface, as shown in Fig. 3(b). Then, it can be seen in Fig. 3(c) that interface crack grows and new delamination appears. With the increase of bending degree, crack initiation is observed in Mg layer in Fig. 3(d). Crack quickly propagates in Mg layer and new parallel crack appears, as shown in Fig. 3(e). Figures 3(f) and (g) are enlarged views of the red rectangle box in Fig. 3(e), which mainly shows the crack tip and secondary crack. It should be noted from cracks (Fig. 3(f)) and slip lines in shear deformation zone (Fig. 3(g)) that crack in Mg layer propagates in the 30° direction.

The same bending experiment is conducted on A300, as shown in Fig. 4(a). It can be seen in Fig. 4(b) that delamination at Al/Mg interface is still the first failure form of annealed laminate.

Therefore, mechanical properties of Ti/Al/Mg/Al/Ti laminate depend on its weak link, i.e., the bonding strength of Al/Mg interface. Figure 4(c) shows the enlarge view of red rectangle box in Fig. 4(b), and four kinds of cracks are observed: (1) cracks at $Al_3Mg_2/Mg_{17}Al_{12}$ interface, which parallels the RD and accounts for the largest proportion; (2) cracks at Al/Al_3Mg_2 interface; (3) cracks at $Mg_{17}Al_{12}/Mg$ interface, which occurs at serrated crack zone; (4) short cracks, parallel to the ND. The first three types are marked by white arrows, and the last one is marked by white ellipses.

With the increase of load, the gap between Mg and Al layers increases, and the short cracks in white ellipses also become wider in Figs. 4(d) and (e). However, no facture occurs in Mg layer under

the same displacement as that of R450. The reason may be that hard and brittle intermetallics in annealed laminate help to bear and release stress.

3.3 In-situ stretching test results

Figure 5 illustrates the whole in-situ stretching test of R450, and the stretching direction is marked in Fig. 5(a). At the early stage, Ti/Al and Al/Mg interfaces are bonded well, as shown in the enlarge view of Fig. 5(b). Then, delamination appears at Al/Mg interface, but there exist some bonded zones, as shown in Fig. 5(c). As stretching test continues, Al/Mg interface presents a complete delamination in Fig. 5(d). It is interesting in Fig. 5(e) that gap
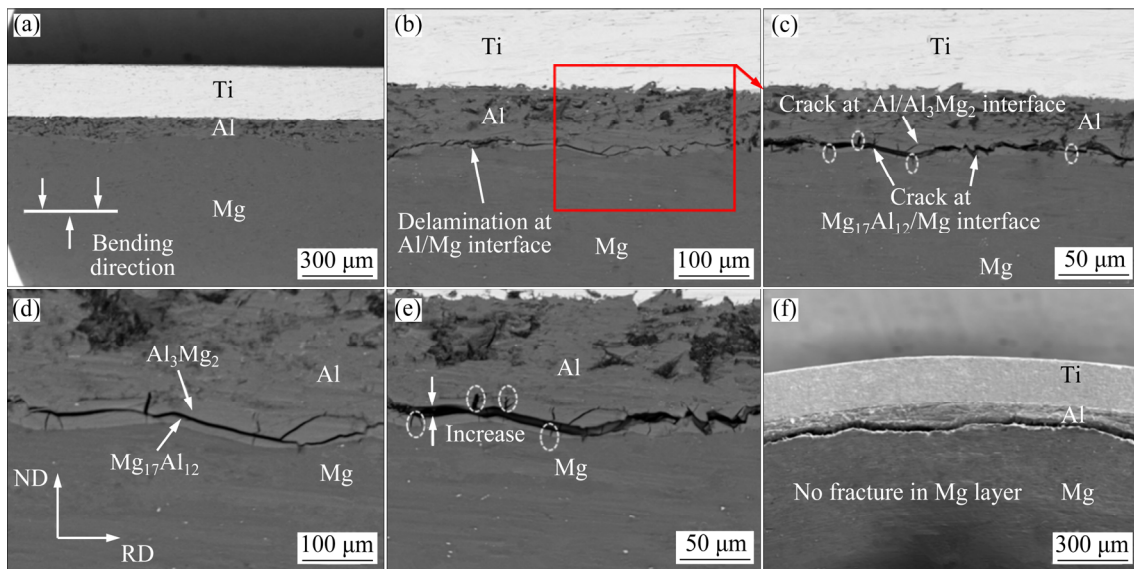
Fig. 4 Microstructure evolution of A300 during in-situ three-point bending
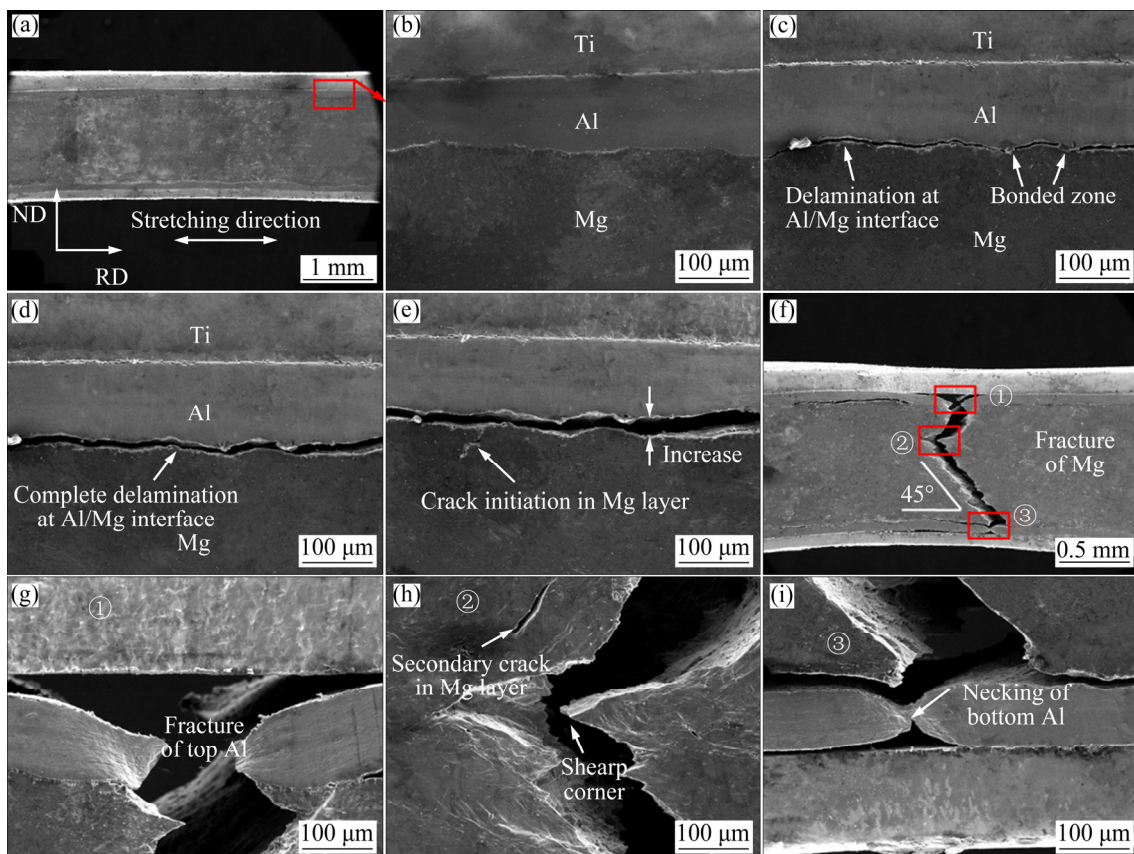
Fig. 5 Microstructure evolution of R450 during in-situ stretching

between Al/Mg interface further increases, and the crack initiation can be found in Mg layer. The crack propagates rapidly until Mg layer completely breaks into two parts in Fig. 5(f), and the angle between stretching direction and crack propagation is around 45°, which is the direction of shear stress during uniaxial stretching.

It should be noted that crack growth in Mg layer is very fast, so the process from Figs. 5(e) to (f) only needs a few seconds. Previous study [27] also proves that once delamination appears, it propagates quickly until the whole laminates fracture. Figures 5(g−i) are partial enlarged views of three red rectangle boxes numbered ①, ② and ③ in Fig. 5(f), respectively, which are beneficial to further studying the specific deformation process of component layers of R450. Combining Figs. 5(g) and (i), it can be found that the top Al layer fractures earlier than bottom Al layer, and Ti layer would be the last broken component layer owing to its highest strength compared with Mg and Al layers.

The specific deformation process is as follows: at the early stage of stretching, five component layers of the laminate experience synchronous elastic and then plastic deformation. Then, synchronous deformation cannot continue due to the difference in ductility between Mg and Al layers. At this time, hindrance of delamination at Al/Mg interface comes from two aspects: (1) the peaks and valleys of wavy interface, which are perpendicular to stretching direction; (2) the friction

at Al/Mg interface. Therefore, the larger the wavy extent of Al/Mg interface is, the later the delamination appears. After delamination appears at Al/Mg interface, the thickness of Al layer in the delamination region determines the fracture time of Al layer. Combining with Fig. 2(a), it can be known that actual cross-sectional area of Al layer in different regions is various during stretching process. The smaller the thickness of Al layer is, the earlier the fracture occurs.

Obviously, fracture of Mg layer results from the combined action of a crack from top zone of R450 and a crack from bottom zone. The top crack and the bottom crack start at the asymmetric locations, propagate separately, and finally converge around the neutral layer of R450, so a sharp corner can be seen in Fig. 5(h). Besides, secondary crack can also be found around the sharp corner of Mg layer.

Crack initiation and propagation of A300 during in-situ uniaxial stretching process are more complicated than those of R450, because of the effect of intermetallics and component layers deformation and their interaction in fracture mode of Ti/Al/Mg/Al/Ti laminate. Hence, intermetallics and component layers are observed, respectively, as shown in Figs. 6 and 7. Moreover, in order to give a comprehensive and detailed presentation of fracture process of A300, the early deformation stage before crack or delamination appeared is omitted.

Figure 6(a) illustrates that delamination occurs locally at the top Al/Mg interface, indicating that
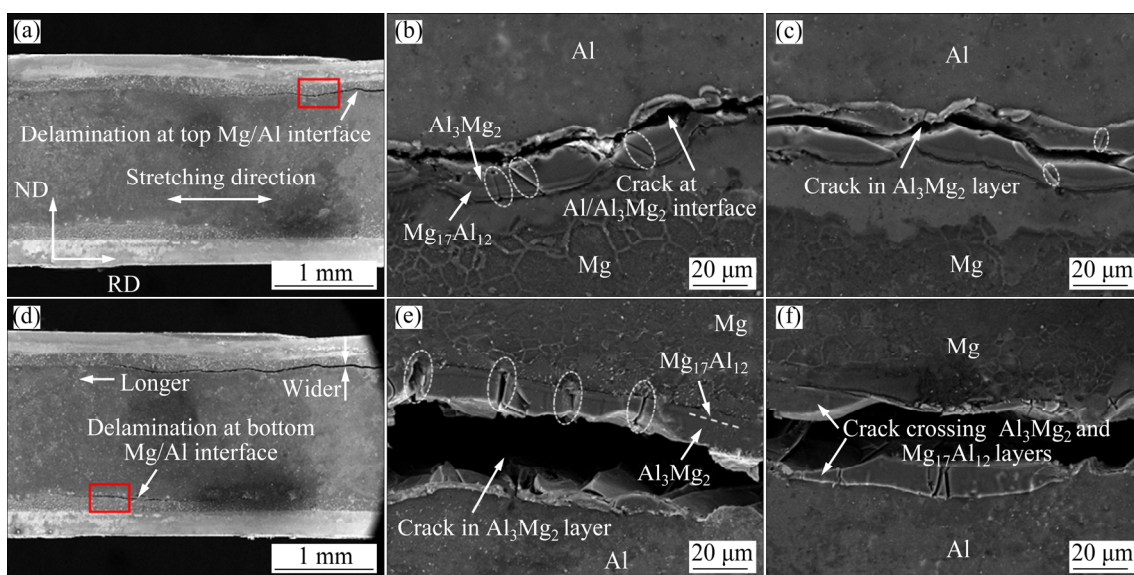
Fig. 6 Intermetallics microstructure evolution of A300 during in-situ stretching

Al/Mg interface delamination is the earliest failure form of Ti/Al/Mg/Al/Ti laminate with or without intermetallics. Figures 6(b) and (c) show the enlarged views of red rectangle box in Fig. 6(a), indicating that cracks at Al/Al$_3$Mg$_2$ interface and in Al$_3$Mg$_2$ itself are the main reason of layer delamination. Besides, short cracks are also found and marked by white ellipses.

As tensile strain increases, delamination at top Al/Mg interface becomes wider and longer, and new delamination at bottom Al/Mg interface appears, as shown in Fig. 6(d). Figures 6(e) and (f) show the enlarged views of red rectangle box in Fig. 6(d). In addition to the crack in Al$_3$Mg$_2$ itself (Fig. 6(e)), a new kind of crack accruing Al$_3$Mg$_2$ and Mg$_{17}$Al$_{12}$ layers is observed in Fig. 6(f). Meanwhile, the width of short cracks parallel to the ND becomes larger (see Fig. 6(e)).

Figure 7 shows the whole fracture process of five component layers of A300, which can be divided into four stages. At stage I, from the delamination gap of top and bottom Al/Mg interfaces in Fig. 7(a), it can be deduced that necking and fracture of component layers of A300 first happen at the severest delamination zone. In-situ stretching of Ti/Al laminate also shows that intermetallics tend to induce microcrack initiation in Ti layer [28]. In its enlarged view (Fig. 7(b)), necking of bottom Al layer can be seen, leading to Al/Ti interface delamination. After a few seconds, bottom Al layer fractures, but Mg layer and bottom Ti layer show no obvious change, as shown in Fig. 7(c).

At stage II, when bottom Al layer completely
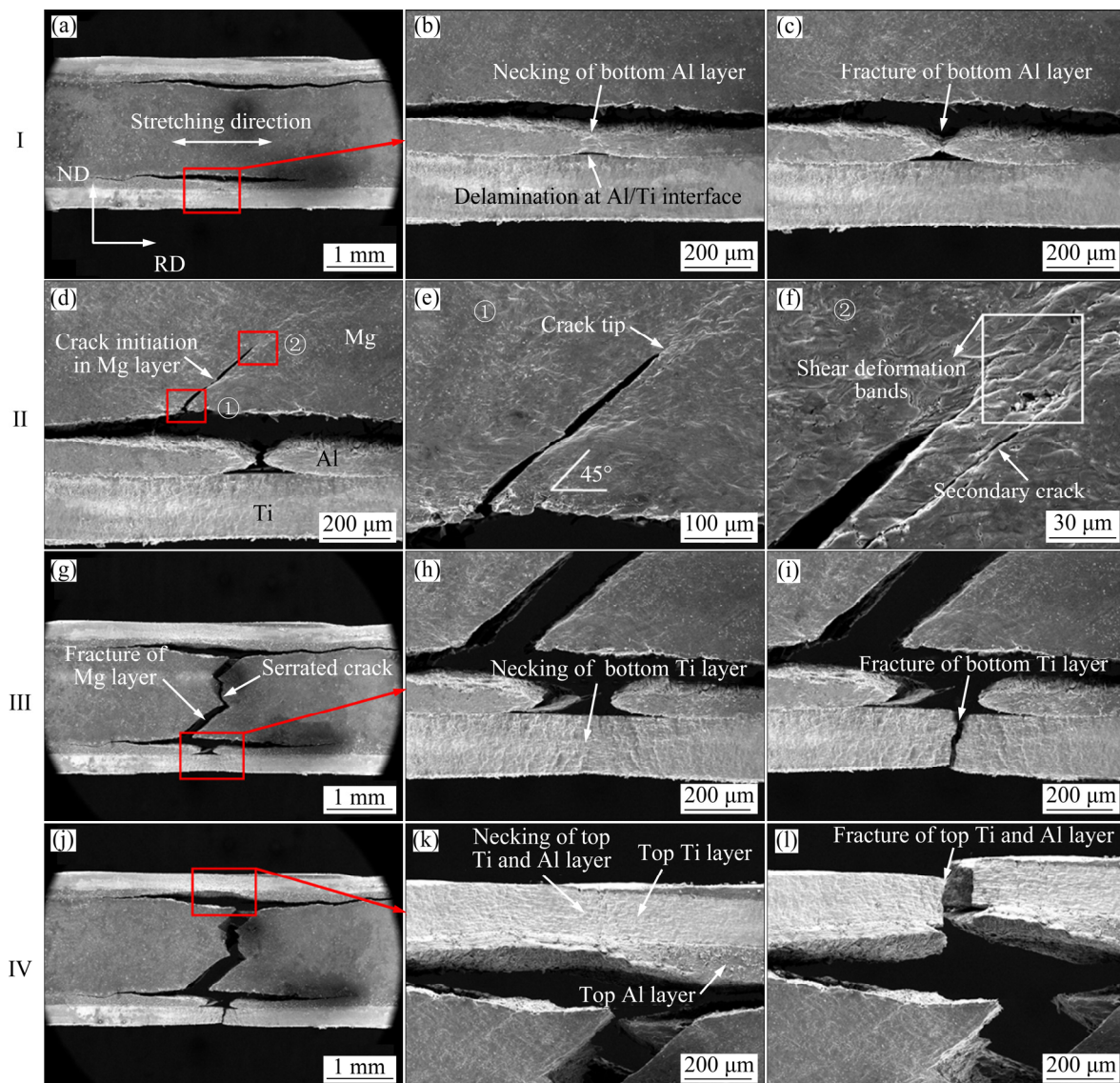
Fig. 7 Microstructure evolution of component layers of A300 during in-situ stretching
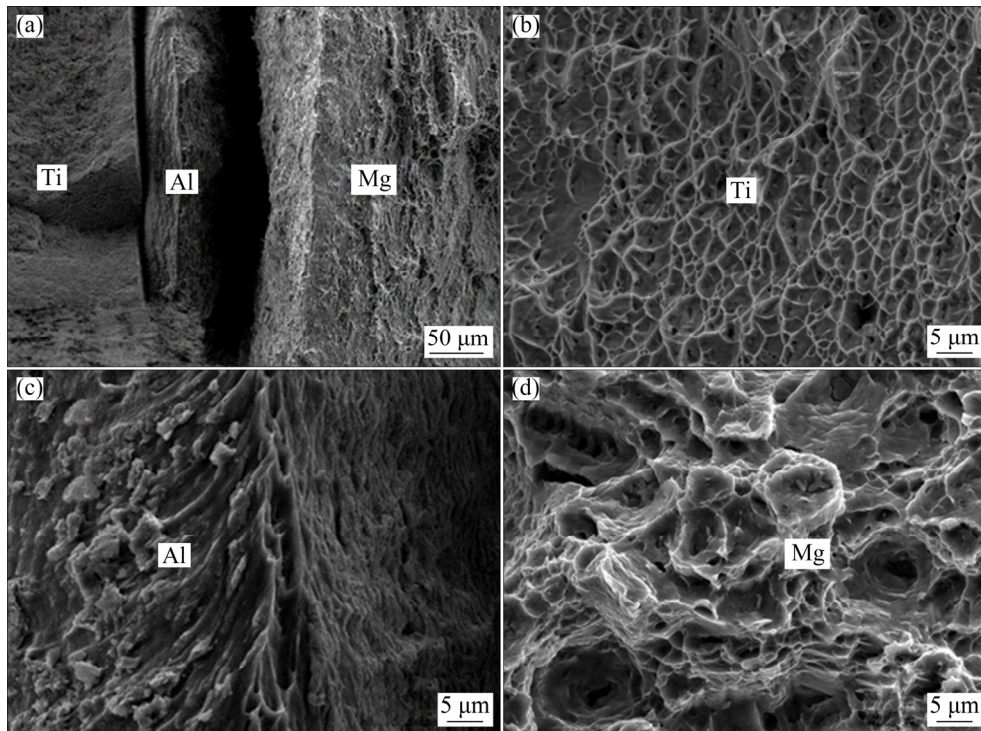
Fig. 8 Microstructure showing fractures of R450 after in-situ stretching: (a) Ti/Al/Mg fracture; (b) Ti layer; (c) Al layer; (d) Mg layer

fractures, crack initiation in Mg layer is found, as shown in Fig. 7(d). Figures 7(e) and (f) show the enlarged views of red rectangle boxes numbered by ① and ② in Fig. 7(d), respectively. Secondary crack and shear deformation zone can be observed around the main crack tip, and an angle of about 45° between stretching direction of crack propagation is also found.

At stage III, Mg layer has been completely broken in Fig. 7(g). According to length of the top crack and the bottom crack in Mg layer, there are reasons to believe that the top crack appears in a short period of time after the bottom crack initiation happens. The serrated crack around the center region of Mg layer is the result of propagation and convergence of the top and bottom cracks. At this moment, the section area of bottom Ti layer decreases, as shown in Fig. 7(h) (enlarged view of red rectangle box in Fig. 7(g)), which indicates that necking happens. After a while, bottom Ti layer fractures (Fig. 7(i)).

At stage IV, it is interesting that the top Al/Ti interface keeps bonding well (Fig. 7(j)) until Al and Ti layers neck (Fig. 7(k)) and fracture (Fig. 7(l)) at the same time. The effective section area of A300 at this stage is too small to bear stretching strain, so

top Ti and Al layers break in a very short time.

Figure 8 gives the fracture of Ti/Al/Mg/Al/Ti laminate. It can be seen in Fig. 8(a) that Ti/Al interface delaminates later than Al/Mg interface, so the gap between Mg and Al layers is much larger than that between Al and Ti layers. All the component layers are characterized by ductile fracture, but they exhibit completely different fractures, as shown in Figs. 8(b−d). Tear ridge can be observed in Al layer. A large number of equiaxed tiny dimples appear on the fracture surface of Ti layer. Comparatively, the size of the dimples of Mg layer is much large and distributed unevenly.

4 Conclusions

(1) Top and bottom Ti/Al and Al/Mg interfaces are bonded well both in R450 and A300, and intermetallics $Mg_{17}Al_{12}$ and Al_3Mg_2 form at the Al/Mg interface. In-situ bending test shows that the crack of intermetallics helps to release stress.

(2) In bending and stretching tests, there exist two kinds of failure forms of R450 and A300. The first is the delamination of Al/Mg interface, and the second is necking and fracture of component layers. However, crack of intermetallics or interface of

intermetallics is the main reason of delamination of Al/Mg interface in A300. Hence, the mechanical properties of Ti/Al/Mg/Al/Ti laminate depend on the bonding strength of Al/Mg interface.

(3) Cracks of intermetallics are complex and irregular in A300. Cracks can be seen at interfaces including $Al_3Mg_2/Mg_{17}Al_{12}$, Al/Al_3Mg_2 and $Mg_{17}Al_{12}/Mg$, in Al_3Mg_2 layer itself, and crossing Al_3Mg_2 and $Mg_{17}Al_{12}$. Besides, some short cracks parallel to the ND are found.

(4) The sequence of necking and facture of component layers is Al, Mg and Ti in most cases, because Al layer has the lowest strength while Ti layer has the highest strength. Angle between crack propagation direction and stretching direction of Mg layer both in R450 and A300 is around 45° due to the effect of shear deformation, and final complete fracture of Mg layer is the result of propagation and convergence of top and bottom cracks.

Acknowledgments

References

[1] SHAN Zhao-hui, BAI Jing, FAN Jian-feng, WU Hong-fei, XU Bing-she. Exceptional mechanical properties of AZ31 alloy wire by combination of cold drawing and EPT [J]. Journal of Materials Science & Technology, 2020, 51: 111−118.

[2] FENG J, LI X W, SUN H F, FANG W B. An ultra-high strength Mg−3Al−Zn alloy with low tension-compression yield asymmetry [J]. Materials Letters, 2020, 269: 127489.

[3] WANG Yang, LIAO Yang, WU Rui-zhi, TURAKHODJAEV N, MARDONAKULOV S. Microstructure and mechanical properties of ultra-lightweight Mg−Li−Al/Al−Li composite produced by accumulative roll bonding at ambient temperature [J]. Materials Science and Engineering A, 2020, 787: 139494.

[4] LIU Yang, MA Yun-zhu, LIU Wen-sheng, HUANG Yu-feng, WU Lei, WANG Tao, LIU Chao, YANG Lun. The mechanical properties and formation mechanism of Al/Mg composite interface prepared by spark plasma sintering under different sintering pressures [J]. Vacuum, 2020, 176: 109300.

[5] WANG Tao, WANG Yue-lin, BIAN Li-ping, HUANG Qing-xue. Microstructural evolution and mechanical behavior of Mg/Al laminated composite sheet by novel corrugated rolling and flat rolling [J]. Materials Science and Engineering A, 2019, 765: 138318.

[6] SADEGHI A, KYOKUTA N, INOUE J, KOSEKI T. Effect of initial texture and microstructure of Mg on mechanical properties of Mg−stainless steel laminated metal composites [J]. Materials Characterization, 2017, 127: 171−178.

[7] HAO Xin-wei, LU Hui-hu, NIE Hui-hui, ZHANG Wang-gang, LI Tao-tao, WANG Tao-lue, LIANG Wei. In-situ investigation of crack initiation and propagation in roll-bonded five-ply ASS/Al/Mg/Al/ASS laminated composites during tensile test [J]. Journal of Alloys and Compounds, 2020, 822: 153608.

[8] HU Xiao-shi, SUN Zhen-ming, ZHANG Chun-lei, WANG Xiao-jun, WU Kun. Microstructure and mechanical properties of bio-inspired Cf/Ti/Mg laminated composites [J]. Journal of Magnesium and Alloys, 2018, 6(2): 164−170.

[9] WANG Yu-hui, KANG Jian-mei, PENG Yan, WANG Tian-sheng, HANSEN N, HUANG Xiao-xu. Laminated Fe−34.5Mn−0.04C composite with high strength and ductility [J]. Journal of Materials Science & Technology, 2018, 34(10): 1939−1943.

[10] CHENG Wen-juan, LIU Yong, ZHAO Da-peng, LIU Bin, TANG Han-chun. Crack propagation behavior of inhomogeneous laminated Ti−Nb metal−metal composite [J]. Transactions of Nonferrous Metals Society of China, 2019, 29(9): 1882−1888.

[11] NING Fang-kun, ZHOU Xiong, LE Qi-chi, LI Xiao-qiang, LI Ying. Fracture and deformation characteristics of AZ31 magnesium alloy plate during tension rolling [J]. Materials Today Communications, 2020, 24: 101129.

[12] ALKAN K, AYTUNA O B, GÜLER B, EFE M. Strong strain path dependence of strain localizations and fracture in magnesium AZ31 sheet [J]. Journal of Magnesium and Alloys, 2020, 8(2): 472−479.

[13] KÖLLNER A, KASHTALYAN M, GUZ I, VÖLLMECKE C. On the interaction of delamination buckling and damage growth in cross-ply laminates [J]. International Journal of Solids and Structures, 2020, 202: 912−928.

[14] JIN Fu-song, XU Peng, XIA Fei, LIANG Hao-feng, YAO Si-shi, XUE Jiang-hong. Buckling of composite laminates with multiple delaminations: Part I. Theoretical and numerical analysis [J]. Composite Structures, 2020, 250: 112491.

[15] SHEN Lu-lu, LIU Ling, WANG Wei, ZHOU Ye-xin. In situ self-sensing of delamination initiation and growth in multi-directional laminates using carbon nanotube interleaves [J]. Composites Science and Technology, 2018, 167: 141−147.

[16] EBRAHIMI S H S, DEHGHANI K, AGHAZADEH J, GHASEMIAN M B, ZANGENEH S. Investigation on microstructure and mechanical properties of Al/Al−Zn−Mg−Cu laminated composite fabricated by accumulative roll bonding (ARB) process [J]. Materials Science and Engineering A, 2018, 718: 311−320.

[17] CHU Qiao-ling, TONG Xiong-wei, XU Shuai, ZHANG Min, YAn Fu-xue, CHENG Peng, YAN Cheng. The formation of intermetallics in Ti/steel dissimilar joints welded by Cu−Nb

composite filler [J]. Journal of Alloys and Compounds, 2020, 828: 154389.

[18] NIE Hui-hui, LIANG Wei, CHEN Hong-sheng, ZHENG Liu-wei, CHI Cheng-zhong, LI Xian-rong. Effect of annealing on the microstructures and mechanical properties of Al/Mg/Al laminates [J]. Materials Science and Engineering A, 2018, 732: 6−13.

[19] GUSSEV M N, LEONARD K J. In situ SEM-EBSD analysis of plastic deformation mechanisms in neutron-irradiated austenitic steel [J]. Journal of Nuclear Materials, 2019, 517: 45−56.

[20] MORTELL D J, TANNER D A, MCCARTHY C T. In-situ SEM study of transverse cracking and delamination in laminated composite materials [J]. Composites Science and Technology, 2014, 105: 118−126.

[21] ZHANG Xing-ru, JIANG Gui-cheng, LIU Dan-qing, YANG Bin, CAO Wen-wu. Improved depolarization behavior and electric properties in (Bi0.5Na0.5)TiO3-based piezoelectric composites[J]. Journal of Alloys and Compounds, 2018, 769: 660−668.

[22] SADEGHI A, INOUE J, KYOKUTA N, KOSEKI T. In situ deformation analysis of Mg in multilayer Mg−steel structures [J]. Materials & Design, 2017, 119: 326−337.

[23] ZHANG Xiao-bo, YU Yang-bo, LIU Bin, ZHAO You-chun, REN Jun-qiang, YAN Ying-jie, CAO Rui, CHEN Jian-hong. In-situ investigation of deformation behavior and fracture

mechanism of laminated Al/Ti composites fabricated by hot rolling [J]. Journal of Alloys and Compounds, 2019, 783: 55−65.

[24] WANG Tao-lue, NIE Hui-hui, MI Yu-jie, HAO Xin-wei, YANG Fan, CHI Cheng-zhong, LIANG Wei. Microstructures and mechanical properties of Ti/Al/Mg/Al/Ti laminates with various rolling reductions [J]. Journal of Materials Research, 2018, 34(2): 1−10.

[25] NIE Hui-hui, HAO Xin-wei, CHEN Hong-sheng, KANG Xiao-ping, LIANG Wei. Effect of twins and dynamic recrystallization on the microstructures and mechanical properties of Ti/Al/Mg laminates [J]. Materials & Design, 2019, 181: 107948.

[26] CHEN Ming-che, HSIEH C C, WU Wei-te. Microstructural characterization of Al/Mg alloy interdiffusion mechanism during accumulative roll bonding [J]. Metals & Materials International, 2017, 13: 201−205.

[27] BENMEDAKHENE S, KENANE M, BENZEGGAGH M L. Initiation and growth of delamination in glass/epoxy composites subjected to static and dynamic loading by acoustic emission monitoring [J]. Composites Science and Technology, 1999, 59: 201−208.

[28] TAO Jie, QIN Liang, WU Qian, WANG Jin, GUO Xun-zhong. In-situ observation of crack initiation and propagation in Ti/Al composite laminates during tensile test [J]. Journal of Alloys and Compounds, 2017, 712: 69−75.

Ti/Al/Mg/Al/Ti 层合板变形行为及断裂形式的原位研究

聂慧慧 [1,2]，郑留伟 [3]，康小平 [4]，郝欣为 [2,5]，李线绒 [2,5]，梁 伟 [2,3,5]

1. 太原理工大学 机械与运载工程学院，太原 030024；
2. 太原理工大学 先进镁基材料山西省重点实验室，太原 030024；
3. 太原理工大学 分析测试中心，太原 030024
4. 山西能源学院，太原 030006；
5. 太原理工大学 材料科学与工程学院，太原 030024

摘 要：为阐明 Ti/Al/Mg/Al/Ti 层合板的变形行为及断裂形式，对轧制态和退火态的层合板进行原位弯曲和拉伸试验，研究组元板和金属间化合物的裂纹萌生和扩展情况。结果表明：无论 Al/Mg 界面有无金属间化合物，Al/Mg 界面分层都是最先出现的断裂形式，因此 Al/Mg 界面结合强度决定层合板的力学性能。在退火态层合板中，金属间化合物中多种多样且无规律的裂纹导致 Al/Mg 界面分层，有助于释放应力。在变形后期，各组元板开始出现颈缩和断裂，依次为 Al 层、Mg 层和 Ti 层。在轧制态和退火态层合板中，在剪切应力作用下，Mg 层裂纹扩展方向与拉伸方向的夹角均为 45°左右，裂纹合并最终导致 Mg 层完全断裂。
关键词：Ti/Al/Mg/Al/Ti 层合板；原位测试；金属间化合物；裂纹萌生；断裂形式

(Edited by Xiang-qun LI)